ROBUST CONTROL DESIGN FOR LOAD REDUCTION ON A LIBERTY WIND TURBINE

Daniel Ossmann, Julian Theis and Peter Seiler
Aerospace Engineering and Mechanics Department
University of Minnesota
Minneapolis, Minnesota, 55455
Email: {dossmann, theis476, seile017}@umn.edu

ABSTRACT

The increasing size of modern wind turbines also increases the structural loads on the turbine caused by effects like turbulence or asymmetries in the inflowing wind field. Consequently, the use of advanced control algorithms for active load reduction has become a relevant part of current wind turbine control systems. In this paper, an H_∞-norm optimal multivariable control design approach for an individual blade-pitch control law is presented. It reduces the structural loads both on the rotating and non-rotating parts of the turbine. Classical individual blade-pitch control strategies rely on single control loops with low bandwidth. The proposed approach makes it possible to use a higher bandwidth since it takes into account coupling at higher frequencies. A controller is designed for the utility-scale 2.5 MW Liberty research turbine operated by the University of Minnesota. Stability and performance are verified using a high-fidelity nonlinear benchmark model.

INTRODUCTION

The size of modern wind turbines has been increasing over the last several years in order to lift wind turbines to a higher power production level. This upscaling goes hand in hand with an increase in structural flexibility and as a consequence also increases the loads on the rotating and non-rotating parts of the turbine. These loads are caused by effects like wind shear, tower shadow, and turbulence. They can have significant impacts on the life cycle of the turbine. The demand of sophisticated control algorithms to actively and robustly mitigate these additional loads has consequently gathered an increased industrial and academic interest.

Classical variable-speed wind turbine control aims to maximize the power output in the different operating regions. Below rated speed, torque control is used to maintain the maximum power output at the maximum extractable power of the flow. Above rated wind speed, collective blade-pitch control is used to limit power production and rotary hub speed to a specified value by pitching all blades to a common angle. Additional algorithms have been developed in the last decade to mitigate different loads on the turbine. In [1], a good overview of possible load mitigation control techniques is provided. For example, filters to damp resonances on the tower bending and the drive-train shaft torsion load are proposed. Further, it is stated that active feedback control of the measured tower acceleration can help to suppress the dynamic tower fore-aft load by collective blade pitch. Modern wind turbines offer the possibility of even more advanced load reduction by means of pitching each blade individually. This individual blade-pitch control can effectively reduce the blade's out-of-plane loads. It requires, however, additional load measurements, either on the rotating or the non-rotating frame [2] and individual actuators on each blade.

Generally, a wind turbine consists of rotating parts (hub, blades, shaft) and non-rotating parts (nacelle, tower, etc.). Thus, its dynamical properties depend on the rotary hub position, which makes a wind turbine a periodic dynamic system. Standard control approaches for linear time invariant (LTI) systems are thus not directly applicable for the design of individual blade-pitch controllers. To overcome this issue, the multi-blade-coordinate

(MBC) transformation was introduced to the wind energy field. The MBC transformation allows the projection of a system's rotating quantities onto non-rotating coordinates. The basic idea of this transformation can be illustrated by an observer in the fixed coordinate frame of the turbine. Instead of experiencing the three blade degrees of freedom individually, the observer experiences their summed effects. For a three bladed wind turbine, these summed effects can be described by the superposition of one symmetric degree of freedom, where all blades bend in the same direction, and two asymmetric degrees of freedom, where the bending of the individual blades is out of phase [3]. The two asymmetric out-of-plane degrees of freedom can be efficiently influenced by individual blade-pitch and are tackled in this paper. Note that due to the non-zero pitch angle of the blades, the out-of-plane degrees of freedom are a combination of edgewise and flapwise degrees of freedoms.

Most state-of-the-art individual blade-pitch controllers make use of MBC-transformed out-of-plane blade load signals and try to mitigate the two asymmetric loads. Two single-input-single-output (SISO) proportional-integral or integral controllers are used to suppress the low frequency components of these loads. The actual blade-pitch commands are then generated by inverse MBC transformation, converting the control signals back to real blade-pitch commands.

Tools have been developed to not only transform the measured signals, but the whole periodic system into the non-rotating frame and approximate it by an LTI model [4]. Analyzing these models shows that the two asymmetric out-of-plane loads are adequately decoupled in the low frequency regime. For exactly this reason, the commonly used two-SISO-loops strategy works is adequate. As the decoupling argument only holds for low frequencies in the fixed frame, such controllers aim only at reducing the static loads in the fixed frame, that correspond to the 1P loads in the rotating frame. The term "P" refers to *per revolution* and indicates multiples of the rotational frequency of the turbine. The dominant (yaw and pitch) loads on the nacelle are located at 3P in the transformed frame. They are difficult to reduce with the classical strategy due to strong coupling effects that appear at higher frequencies.

Approximating the periodic model with an LTI model also enabled the application of sophisticated, model-based control approaches. Multivariable control designs were investigated in [2] based on a linear quadratic regulator and in [5] based on H_∞-norm optimal control. Both controllers were shown to yield similar results as the classical two-SISO-loops strategy. One main aspect not addressed in these articles is the fact that multivariable control can be used to increase the controller bandwidth beyond what is possible with the classical strategy. The controller can then not only mitigate the static load, but also the 3P load in the MBC-transformed system. Thus in this paper, a multivariable control design approach and a clear and distinct tuning strategy for a controller that can mitigate both dominant blade and nacelle loads is presented. The control strategy is applied to the linearized model of the Clipper Liberty C96 research turbine operated by the University of Minnesota. The ultimate goal is to test the H_∞ controller on the real turbine in the near future.

MULTIBLADE COORDINATE TRANSFORMATION

The MBC transformation is used to transform quantities from the rotating frame to the non-rotating frame. For example, the three out-of-plane degrees of freedom of the individual blades can be transformed to the fixed frame, where they result in a collective degree of freedom, in which all blades move synchronously fore, and aft and two asymmetric degrees of freedom, in which the blades move asymmetrically fore and aft. Similar physical explanations can be found for the in-plane motions of the blades [3]. This paper focuses on the blades' out-of-plane degrees of freedom, as they can be effectively influenced with individual blade-pitch control.

For a better understanding of the MBC transformation, a short review is given in this section. The transformation matrix from the rotary frame to the fixed frame is defined by

$$T(\phi) = \frac{2}{3}\begin{bmatrix} 1/2 & 1/2 & 1/2 \\ \cos(\phi) & \cos(\phi+\frac{2}{3}\pi) & \cos(\phi+\frac{4}{3}\pi) \\ \sin(\phi) & \sin(\phi+\frac{2}{3}\pi) & \sin(\phi+\frac{4}{3}\pi) \end{bmatrix}, \qquad (1)$$

where ϕ is the rotary position of the first blade. The out-of-plane loads M, measured on the three blades, can be transformed with (1) to the non-rotating frame, resulting in one symmetric and two asymmetric loads [3]. The symmetric load is strongly connected to the thrust of the turbine, which is a byproduct of the moment (and power) generation. It can be effectively controlled via collective blade-pitch. Individual blade-pitch, on the other hand, can be efficiently used to mitigate the two asymmetric loads that appear as a pitch moment $M_{\cos}$ and a yaw moment $M_{\sin}$ on the nacelle in the fixed frame. Using the shorthand notation

$$V^T(\phi) = \begin{bmatrix} \cos(\phi) & \cos(\phi+\frac{2}{3}\pi) & \cos(\phi+\frac{4}{3}\pi) \\ \sin(\phi) & \sin(\phi+\frac{2}{3}\pi) & \sin(\phi+\frac{4}{3}\pi) \end{bmatrix} \qquad (2)$$

for the last two rows of the matrix in (1), these cyclic moments are expressed in terms of the individual blade moments as

$$\begin{bmatrix} M_{\cos} \\ M_{\sin} \end{bmatrix} = \frac{2}{3} V^T(\phi) \begin{bmatrix} M_1 \\ M_2 \\ M_3 \end{bmatrix}. \qquad (3)$$

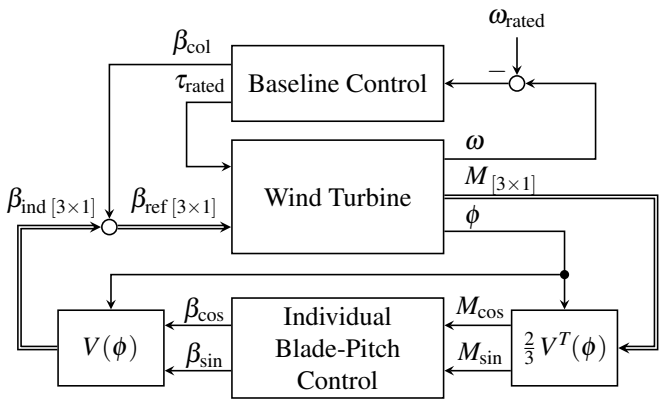

FIGURE 1. Control architecture for individual blade-pitch control.

FIGURE 2. UMN's research turbine [6].

The inverse of the MBC transformation is given by

$$T^{-1}(\phi) = \begin{bmatrix} 1 & \cos(\phi) & \sin(\phi) \\ 1 & \cos(\phi + \frac{2}{3}\pi) & \sin(\phi + \frac{2}{3}\pi) \\ 1 & \cos(\phi + \frac{4}{3}\pi) & \sin(\phi + \frac{4}{3}\pi) \end{bmatrix}. \tag{4}$$

This transformation is required for the implementation of an individual blade-pitch controller, designed in the MBC-transformed reference frame. The two cyclic control signals $\beta_{\cos}$ and $\beta_{\sin}$, generated by the controller, need to be transformed back into three blade-pitch angles using the second and third column of (4). This again is more conveniently expressed as

$$\begin{bmatrix} \beta_1 \\ \beta_2 \\ \beta_3 \end{bmatrix} = V(\phi) \begin{bmatrix} \beta_{\cos} \\ \beta_{\sin} \end{bmatrix}. \tag{5}$$

The individual blade-pitch commands β_{ind} are added to the collective pitch command β_{col}, which is generated by the baseline control law from the rotational speed ω and its rated value ω_{rated}. The complete control architecture is depicted in Fig. 1 including the region 3 rated generator torque command τ_{rated}.

To be able to implement individual blade-pitch control, individual actuators and load sensors need to be available for each blade. On the Liberty wind turbine the load sensors are installed at the blade roots, which is accounted for in the controller design.

CLIPPER WIND TURBINE

The wind turbine considered in this paper is the utility-scale three-bladed Clipper Liberty 2.5 MW research turbine of the EOLOS Wind Energy Research Consortium located at the UMore Park in Rosemount, MN, and shown in Fig. 2. It has a hub height of 80 m and a rotor diameter of 96 m. It is common to classify the operating range into standstill (region 1), variable speed (region 2), and constant speed (region 3). The turbine's cut-in wind speed is 3 m/s, from which on a $k\omega^2$ feedback is used to control the generator torque. The range from 8 to 12 m/s is used to transition between the control laws of region 2 and region 3 and is referred to as region 2.5. The rated region 3 operation starts at about 12 m/s. A scheduled proportional-integral baseline control law is used in this region to maintain rated rotor speed and moment via collective blade-pitch. The turbine cuts out at a wind speed of 25 m/s.

Nonlinear Model

An industrial high-fidelity nonlinear simulation model of the Clipper wind turbine in the Fatigue, Aerodynamics, Structures, and Turbulence (FAST) simulator [7] is used. The overall model features a detailed structural model with various degrees of freedom of the turbine and simulates steady aerodynamics. Linear first order models for actuators and sensors are included. The generator dynamics are neglected, as the power electronics on modern utility-scale wind turbines ensure a much faster torque response time than encountered in the rest of the system. The model is augmented with the certified Clipper baseline control law for the different wind regimes as described above. This baseline law includes protection functions that reduce the torque and power overshoots in region 3 in case of turbulence.

Linear Model

The FAST code provides algorithms to trim the model around a defined operating point and to derive linearized models for different rotary positions [7]. In this way, a periodic state space model in a gridded format is available. The model is of 17$^{\text{th}}$ order and includes the rotary shaft velocity, four states describing the tower fore-aft and side-to-side flexibility, as well as six states to describe the first flapwise bending and six states to describe the first edgewise bending of the blades in the rotary frame.

The MBC transformation cannot only be applied to signals but also allows the conversion of a periodic state space model from a rotating into a non-rotating coordinate system. The derivation of the state transformation is not provided here due to a lack of space, but interested readers find clear derivations in [4,8]. As for the signals, the flapwise and edgewise states are transformed to symmetric and asymmetric states, also referred to as collective and cyclic states [3]. While the MBC transformation still results in a periodic system, analyses have shown that this transformed system can be approximated well by an LTI model obtained from averaging over the rotary position [4]. Such an LTI model serves as the design model for the individual blade-pitch controller in this paper. Its inputs are the cyclic pitch commands $\beta_{\cos}$ and $\beta_{\sin}$ as defined in (5) and its outputs are the cyclic moments $M_{\cos}$ and $M_{\sin}$ as defined in (3). It can be shown that cyclic pitch commands do not influence the collective load of the turbine. This is an important fact, as the individual blade-pitch control algorithm should not change the thrust and the torque of the turbine in order to maintain the power output at its desired level.

The wind turbine model is linearized for different wind speeds along the baseline controller scheduling trajectory, defined by generator torque and blade pitch angle. Fig. 3 depicts the poles of the resulting LTI model in dependence on the wind speed. The pole near the origin corresponds to the rotary velocity of the turbine and nearly acts as a pure integrator. The tower's first side-to-side and fore-aft modes at around 2 rad/s show low damping but remain almost constant over the wind speed. The flapwise modes increase in frequency in the region 2 and 2.5 operation. After the rated rotation speed of the turbine is reached, the damping of these modes increases with increasing wind speed while the frequency remains unchanged. The red lines in the figure represent the 1P and 3P frequencies of the turbine in region 3. One of the flapwise modes and one of the edgewise modes can be seen to approach the 3P frequency. An overlapping of the turbine modes with these frequencies potentially causes problems, as normal operation of the turbine excites dynamics at these frequencies. The flapwise mode that approaches the 3P frequency is considered safe, as it is rather well damped. The edgewise mode, on the other hand, is likely to cause unwanted effects in region 3, due to its poor damping. The third edgewise mode is located around 13 rad/s and is not shown in the figure.

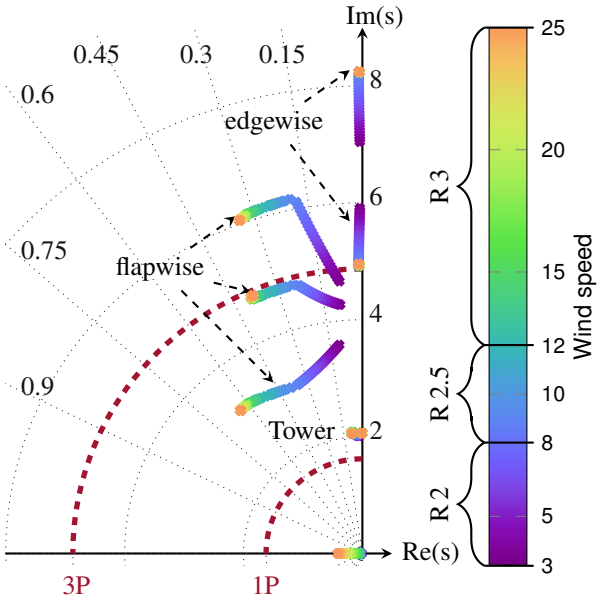

FIGURE 3. Pole migration for variation in the wind speed.

MULTIVARIABLE CONTROL LAW DESIGN

The MBC-transformed and averaged Clipper model at a fixed wind speed of 12 m/s is used as the design model. This wind speed was chosen as design point as it was possible to design a controller providing closed loop stability in the whole region 3 operating region. Fig. 4 shows the Bode plot from cyclic blade-pitch commands to cyclic moments, normalized by the DC-gains of the diagonal elements. These cyclic moments induce yaw and pitch loads on the nacelle. Notably, the off-diagonal elements have magnitude values of around -10 dB in the low frequency range. For the design of classical individual blade-pitch controllers with two SISO integral control loops, this value is considered sufficiently small to neglect cross coupling, although it is far from perfect decoupling. When trying to actively mitigate

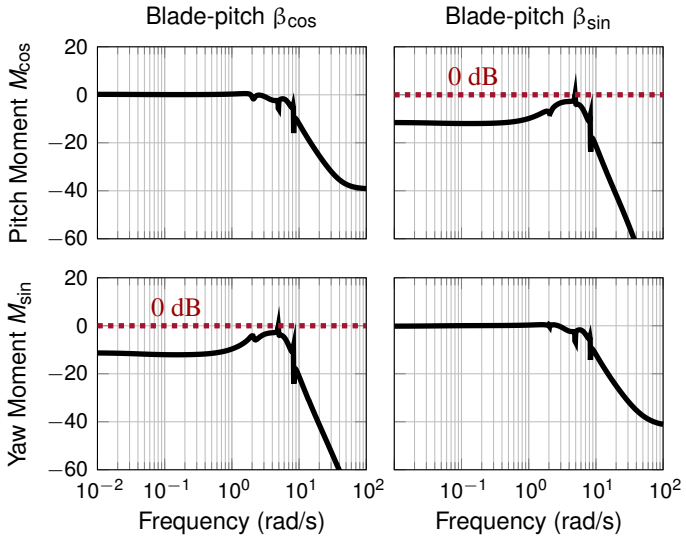

FIGURE 4. Normalized Bode magnitude plot of the 2-by-2 design system from the cyclic pitch commands to the yaw and pitch moments on the nacelle for 12 m/s wind speed.

the loads at higher frequencies, the coupling becomes more important with magnitudes comparable to and even above those of the diagonal elements. This observation is the main motivation for the use of multivariable control to achieve load reduction at larger frequencies.

The 1P load in the rotating frame mainly translates to a constant contribution in the fixed frame. The classical two-integral-loops approach makes use of this and achieves 1P load reduction in the rotating frame by aiming at the constant load in the fixed frame. In terms of the MBC-transformed and averaged system, this can be thought of as a sensitivity reduction at zero frequency. The 2P load in the rotating frame shows up mainly as a 3P load in the fixed frame. Adapting the control strategy to also reduce these 2P loads thus involves sensitivity reduction both at zero and at the 3P frequency in the fixed frame. H_∞ control is particularly useful for this task, since it allows the designer to directly "shape" the closed-loop frequency response to meet these requirements.

H_∞ Control Design

The H_∞-norm of an LTI system $H(s)$ from input d to output e is defined as

$$\|H(s)\|_\infty = \sup_\omega \bar{\sigma}(H(j\omega)) = \sup_{d\in L_2\setminus\{0\}} \frac{\|e\|_2}{\|d\|_2}, \tag{6}$$

where $\bar{\sigma}(\cdot)$ denotes the largest singular value. This norm measures the maximum gain of $H(s)$, i. e., the largest amplification of L_2 input signals over all frequencies and input/output directions. The control problem is formulated as the closed-loop interconnection shown in Fig. 5 and performance is measured by the H_∞-norm from $d = \left[\begin{smallmatrix} d_1 \\ d_2 \end{smallmatrix}\right]$ to $e = \left[\begin{smallmatrix} e_1 \\ e_2 \end{smallmatrix}\right]$. The corresponding transfer function is

$$\begin{bmatrix} e_1 \\ e_2 \end{bmatrix} = \begin{bmatrix} W_u & \\ & W_e \end{bmatrix} \begin{bmatrix} -T_i & KS_\mathrm{o} \\ -GS_\mathrm{i} & S_\mathrm{o} \end{bmatrix} \begin{bmatrix} W_1 & \\ & W_2 \end{bmatrix} \begin{bmatrix} d_1 \\ d_2 \end{bmatrix}. \tag{7}$$

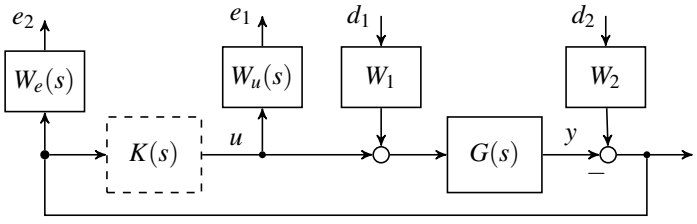

FIGURE 5. Generalized plant interconnection for the individual blade-pitch H_∞ control design.

In (7) and in the following, the dependency on the Laplace variable s is not stated explicitly to shorten notation. The plant model is denoted G, K is the controller, $S_\mathrm{o} = (I + GK)^{-1}$ is the output sensitivity function, $S_\mathrm{i} = (I + KG)^{-1}$ is the input sensitivity function, and $T_\mathrm{i} = KG(I + KG)^{-1}$ is the complementary input sensitivity function [9]. Further, KS_o is called control sensitivity and GS_i is called disturbance sensitivity. A dynamic controller K that ensures stability of the closed loop and guarantees an upper bound on the H_∞-norm from d to e can be synthesized by solving two Riccati equations [9, 10]. Synthesis algorithms that seek to minimize the upper bound are readily available, e. g., in the Matlab Robust Control Toolbox [11].

Closed Loop Shaping Strategy

The crucial part of the design is to select weights that impose a desired loop shape on the four sensitivity functions. Two cyclic loads are fed back to generate two cyclic command signals. Thus, all weightings are 2-by-2 matrices. There is, however, no apparent reason to use different weights for the individual channels and hence the matrices are selected as $W_1 = w_1 I_2$, $W_2 = w_2 I_2$, $W_e = w_e I_2$ and $W_u = w_u I_2$. Static weights w_1 and w_2 are used at the disturbance inputs.

The ratio $\frac{w_1}{w_2}$ determines the importance of rejecting input disturbances over output disturbances. For the present design, it is chosen as 10 to emphasize the importance of rejecting input disturbances. The weights are consequently selected as $w_1 = 10$ and $w_2 = 1$. The filter w_u penalizes the controller output with the goal to limit control effort. Further, high frequency control action that may result in reaching the rate limits of the actuators should be avoided. Thus, w_u is selected with a high gain at frequencies beyond the actuator bandwidth and a low gain for frequencies below the actuator bandwidth. For the Clipper Liberty turbine, the actuator bandwidth is 10–15 rad/s and so w_u is selected with a 0 dB crossing at 6 rad/s in order to reduce control authority above this frequency. The controller is consequently forced to roll off below the actuator bandwidth. The filter w_e is weights the control error, i. e. it shapes the sensitivity and disturbance sensitivity functions. A high gain of w_e at a given frequency dictates a sensitivity reduction at that frequency, which results in high controller gains and improves disturbance rejection. Since the constant load in the fixed frame needs to be suppressed analog to the classical integral control strategy, the weight is selected to have a high gain in the low-frequency range up to 0.3 rad/s. Additionally, the controller should actively suppress the loads at the 3P frequency of about 4.8 rad/s. Thus, additional penalty is added in the vicinity of the 3P frequency by multiplying the low frequency weight with an inverse notch filter, tuned to that frequency. Fig. 6 shows magnitude plots of the weighting filters. Their transfer functions

are

$$w_u = 500\,\frac{s+3.464}{s+3464}$$
$$w_e = 0.1\,\frac{s+3}{s+0.03}\,\frac{s^2+0.49s+24}{s^2+6.93s+24}. \tag{8}$$

The reduction in the disturbance sensitivity is confirmed by the singular value plot depicted in Fig. 7. For low frequencies (<0.8 rad/s) and around the 3P (≈4.8 rad/s), the magnitude of the closed loop lies clearly below the open loop plot. As an inevitable consequence of Bode's sensitivity integral [9, 12], the sensitivity is increased between 0.8 rad/s and 4 rad/s. In the high frequency regime above roughly 5 rad/s, the open loop and closed loop are indistinguishable. This confirms the low control activity beyond that frequency.

The Bode plot of the resulting controller is depicted in Fig. 8. It feeds back the MBC-transformed out-of-plane blade loads $M_{\cos}$ and $M_{\sin}$ to the cyclic pitch commands $\beta_{\cos}$ and $\beta_{\sin}$. In the low-frequency range, the diagonal elements are dominant. Around the 3P frequency, the off-diagonal elements have a comparably large magnitude. This is an important aspect of the proposed multivariable control law, as these couplings are ignored by the classical individual blade-pitch control design that consequently only works at low frequencies.

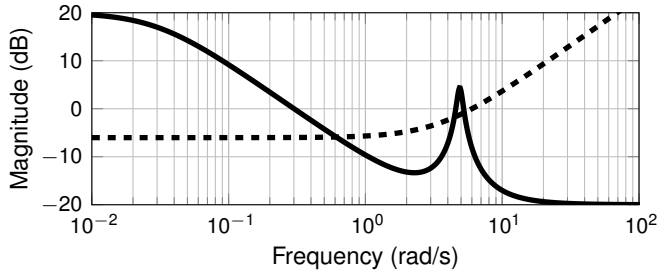

FIGURE 6. Selected filter weights w_e (——) and w_u (- - -).

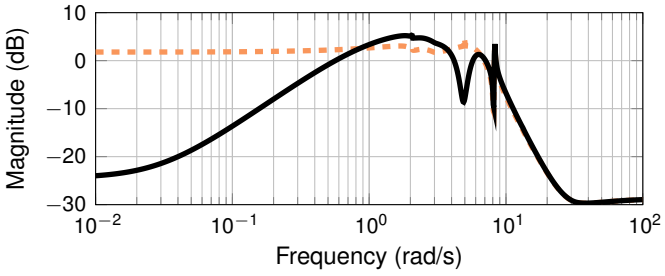

FIGURE 7. Singular value plot of the disturbance sensitivity for the open (- - -) and closed loop (——).

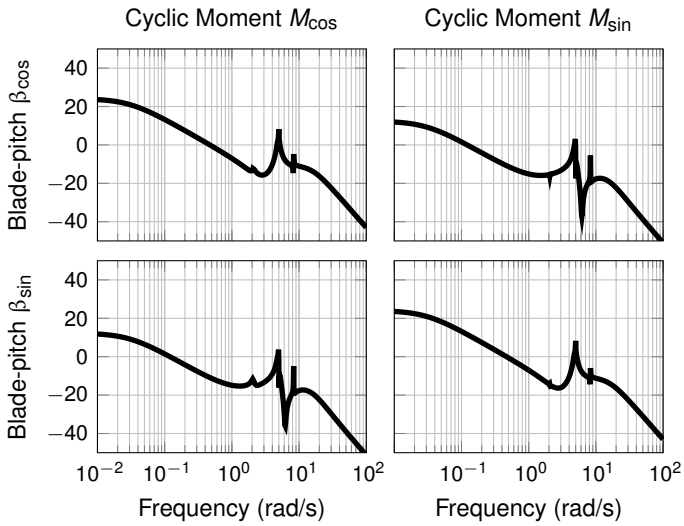

FIGURE 8. Bode magnitude plot of the controller.

VERIFICATION

For the verification process of the designed controller, stability margins at the design point of 12 m/s wind speed are calculated. The dependency of these margins on the wind speed is determined in the whole operational region 3. Nonlinear simulation is used to derive damage equivalent loads and verify the load reduction capabilities of the controller.

Robustness Margins

The most common metric to quantify robustness for a control system is given by the classical gain and phase margins. The former specifies how much gain variation a single loop-transfer function can tolerate before instability occurs. The second measures the amount of phase loss that this loop can tolerate. Both margins are independent of each other. There are different specifications depending on the application field. For example, stringent certifications requirements in aerospace require at least 6 dB gain margin and 60 deg phase margin. These requirements also serve as a basis for the controller analysis in this paper. While these margins are of great practical importance, they can overlook destabilizing combinations of gain and phase that independently are considered safe. It is therefore important to also take into account simultaneous gain and phase variations. The corresponding metric is known as disk margin and can be calculated from $S_i - T_i$ and $S_o - T_o$, where T_o is the output complementary sensitivity function, for the inputs and the outputs of the plant, respectively [13]. They are easily extended to the multivariable case, allowing for simultaneous perturbation of several loops. An input-output disk margin is obtained by breaking the loops at all inputs and all outputs at the same time, considering simultaneous perturbation of all signals. This is the most conservative approach

to analyze the stability margins. It may seem overly conservative for the example in this paper, as the same type of load sensors and actuators are used in each of the four loops. It is, however, a valuable certificate for robustness of the system.

The resulting worst case of the classical gain and phase margins over the four SISO loops (two loops result from break points at the plant inputs, two from break points at the outputs) yields 11.8 dB and 76 deg. The worst case single-loop disk margin is 11.3 dB and 60 deg, indicating a highly robust system against single loop uncertainties. Finally, the multiple loop analysis results in a disk margin of 5.2 dB and 32 deg, which further supports the indication of high robustness. Note, a margin of above 3 dB is considered an acceptable level of degradation with respect to the single-loop margins. Encouraged by these results, the change of the margins with the change in wind speed is calculated. Wind speed variation in the operational region 3 of the Clipper turbine is rather large, lying between 12 and 25m/s.

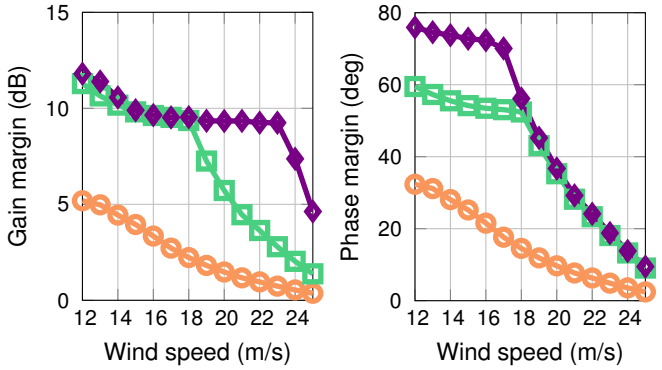

FIGURE 9. Determined classical (—◆—), disk (—□—) and multi-input multi-output (—○—) margins of the designed controller over wind speed.

The margins decrease when moving away from the design point but the system remains stable for all operating conditions. While until about 18 m/s, the disk margins stay in a satisfactory range, above 18 m/s a sharp decrease is observed. The worst case single-loop disk margin decreases to 1.5 dB and 10 deg, which is clearly unsatisfactory. The cause for this is revealed when looking at the critical frequency at which the worst case margins are attained. At wind speeds below 18 m/s, the critical frequency lies around 2 rad/s, while at wind speeds above 18 m/s, the critical frequency lies close to 3P. At the 3P frequency, one of the lightly damped asymmetric edgewise modes is located (see Fig. 3). With increased blade-pitch angle, the out-of-plane motion of the blades contains a larger contribution from the edgewise degree of freedom at higher wind speeds, where the blade-pitch angle is larger. This increasing contribution shows up as a peak in the singular value plots, which consequently decreases the margins at that frequency. It could thus be advantageous for robustness to design different controllers for different wind speeds and to use gain-scheduling or linear parameter-varying control techniques in future work.

Nonlinear Simulation

The developed controller is first tested for the design wind condition at 12 m/s using the nonlinear FAST model of the Clipper turbine. A turbulence level of 7 % in all three directions is applied. The wind field has been generated using the freely available Turbsim software [14]. A state-of-practice individual blade-pitch controller is used for comparison. The controller consists of two decoupled SISO integral compensators of the form $\frac{0.001}{s}$, leading to an open loop bandwidth (0dB crossing) at around 0.25 rad/s. From the resulting simulation data, the damage equivalent loads (DELs) are calculated using the freely available software tool MCrunch [15]. The method of calculating DELs simplifies the process of producing fatigue test loads from a design load spectrum, as it can be done without specific knowledge of the blade structure or geometry. The only inputs needed are the fatigue-load spectrum and fatigue properties of the material [16]. The DELs represent a measure of equivalent fatigue damage caused by each load and take into account material properties [2]. In this work, S-N slopes of 4 and 10 are used, representative for typical steel and composite materials.

From the time series of the yaw bearing moment in Fig. 10, it can already be seen that the multivariable controller results in less excitations not only compared to the baseline controller, but also to the classical two-integral-loops controller.

Further insight is obtained when power spectral densities (PSD) are considered. Fig. 11 depicts the PSD of the blade bending moment for a wind speed of 12 m/s with a turbulence of 7 % in all three directions. The simulations results for the baseline controller without individual blade-pitch control show a high peak at the 1P frequency around 1.6 rad/s. Around the 2P frequency (4.8 rad/s), an increased loading is present, which can be seen in the lower diagram. In comparison, the classical individual blade-pitch controller that uses two integral feedback loops is able to mitigate the 1P load very well. The multivariable controller developed in this paper also achieves this reduction in the 1P load but additionally also reduces the 2P loads on the blades.

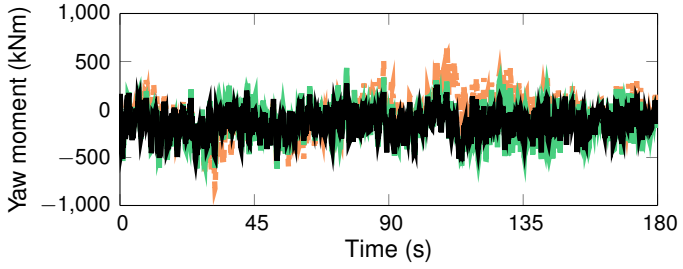

FIGURE 10. Time series of yaw bearing yaw moment for baseline (- - -), two integral loops (——), and H_∞ controller (——).

The reduction of loads at higher frequencies is confirmed when analyzing the loads that act on the non-rotating frame, namely the yaw and pitch loading on the nacelle in Fig. 12. The 1P blade loads appear as a constant load in the non-rotating frame, which is clearly visible in the diagrams of Fig. 12. Just as the 1P load on the blades, this load is mitigated well by both individual blade-pitch controllers. The 2P load on the blades produces a dominant 3P load in the fixed frame. This load is suppressed only by the multivariable controller.

Suppressing this load of course requires higher activity of the blade pitch actuation system, depicted in Fig. 13. For low frequencies (<0.6 rad/s), all three controllers provide the same pitch action, which is due to the dominance of the baseline control law, commanding collective pitch action. Around the 1P frequency, both individual blade-pitch controller show an increased control action in order to mitigate the constant load on the nacelle. The multivariable controller shows a large 2P control component that is required to mitigate the 2P blade loads and the 3P nacelle loads. Note that the y-axis of the plot is in log scale.

To quantify the improvements, the damage equivalent loads on the blades and the nacelle are computed. Table 1 presents the loads using the baseline control law alone, with classical and with H_∞ individual blade-pitch control. Both, the two loop integral and the H_∞ controller are able to reduce the out-of-plane bending moment on the blades. While the two integral feedback loops mainly suppress the constant load in the fixed frame, the H_∞ individual blade-pitch controller works over a wider frequency range and can therefore reduce the loads even more.

	Baseline	**Integral**		H_∞	
Blades					
in-plane	3196	3169	-1 %	3431	+7 %
out-of-plane	1018	766	**-24 %**	667	**-34 %**
Nacelle					
yaw	516	511	-1 %	395	**-24 %**
pitch	454	472	+4 %	347	**-23 %**
Tower					
side-to-side	4447	4395	-1 %	4776	+7 %
fore-aft	2852	2772	-3 %	2689	-6 %
Shaft					
bending (y)	480	501	+5 %	344	**-28 %**
bending (z)	487	483	-1 %	342	**-30 %**

TABLE 1. Damage equivalent loads (kN) based on simulation results.

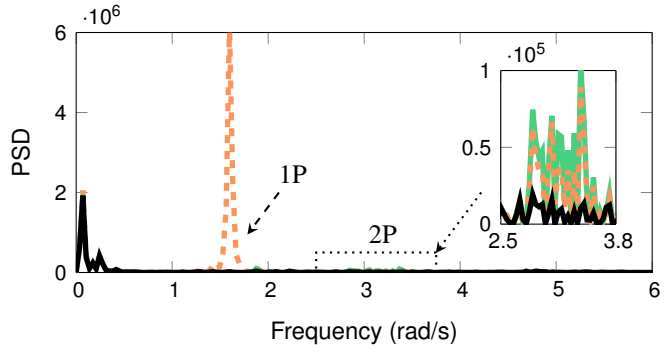

FIGURE 11. Power spectral density of the blade bending moment for baseline (- - -), two integral loops (——), and H_∞ controller (——).

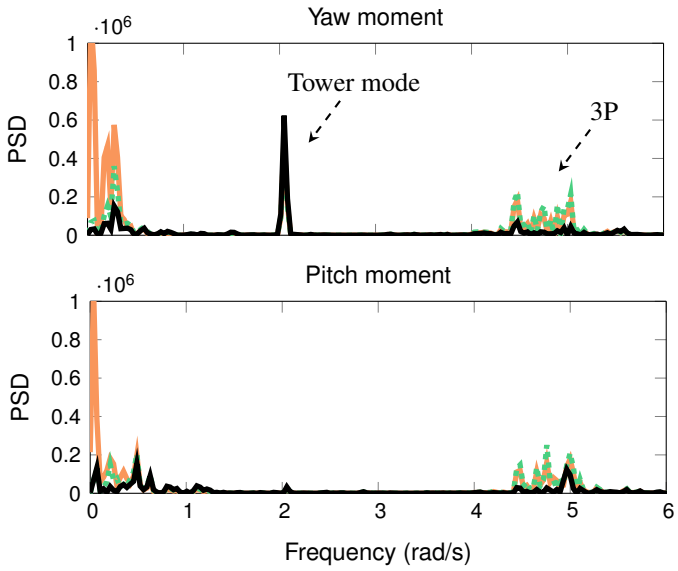

FIGURE 12. Power spectral density of the nacelle moments for baseline (- - -), two integral loops (——), and H_∞ controller (——).

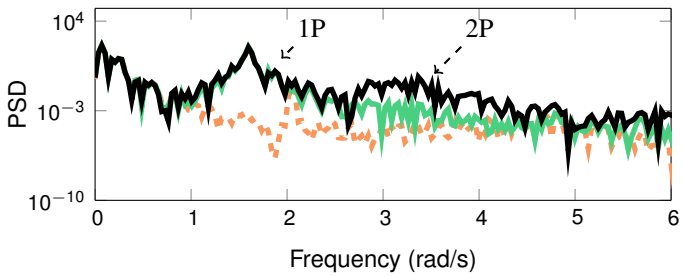

FIGURE 13. Power spectral density of commanded blade-pitch for baseline (- - -), two integral loops (——) and H_∞ controller (——).

The main advantage of the H_∞ individual blade-pitch controller becomes clear when the pitch and yaw loads on the nacelle are considered. Due to the control activity around the 3P frequency, these loads can be reduced by about 30 %, while the classical individual blade-pitch controller lets these loads unchanged. Finally the controller is tested at higher winds speeds in region 3, namely at 16 m/s, 20 m/s and the maximum wind speed of 25 m/s. Although the robustness margins are lower as presented above, the load reduction capabilities are confirmed on these wind speeds and result in similar percentages as on the design point of 12 m/s, as depicted in Fig. 14. The power production is influenced below 0.8 % by the proposed individual blade-pitch controller at the tested wind speeds, confirming the decoupling of individual and collective blade-pitch control.

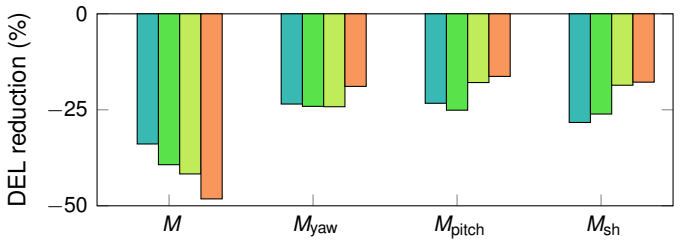

FIGURE 14. Achieved load reduction for the blade out-of-plane load M, the nacelle's yaw M_{yaw} and pitch moment M_{pitch}, and the shaft bending moment around the y-axis M_{sh} at 12 m/s ( ), 16 m/s ( ), 20 m/s ( ), and 25 m/s ( ).

CONCLUSION

A multivariable control design approach for an individual blade-pitch control law to reduce structural loads on the rotating and non-rotating parts of a turbine has been presented. The presented approach overcomes the limitation of the classical single loops control strategy that, due to an inherent coupling at higher frequencies, can only be designed for low frequencies. The proposed procedure has been successfully applied to the to utility-scale 2.5 MW research turbine operated by the University of Minnesota. Performance and stability of the wind turbine augmented with the proposed controller was verified in industrial nonlinear high-fidelity simulations.

ACKNOWLEDGMENT

This work was performed in the framework of the Xcel Energy Renewable Energy Fund: Contract Number RD4-13. The project title is *Virtual Wind Simulator with Advanced Control & Aeroelastic Model for Improving the Operation of Wind Farms*.

REFERENCES

[1] Bossanyi, E., 2000. "Development in closed loop controller design for wind turbines". In ASME Wind Energy Conference, pp. 64–74.

[2] Bossanyi, E., 2003. "Individual blade pitch control for load reduction". *Wind Energy,* ***6***(2), pp. 119–128.

[3] Bir, G., Wright, A., and Butterfield, C., 1997. "Stability analysis of a variable-speed wind turbine". In Proc. ASME Wind Energy Symposium, no. 97-0965.

[4] Bir, G., 2008. "Multi-Blade Coordinate Transformation and its Application to Wind Turbine Analysis". In Proc. of 46th AIAA Aerospace Sciences Meeting and Exhibit, no. 2008-1300.

[5] Geyler, M., and Caselitz, P., 2008. "Robust Multivariable Pitch Control Design for Load Reduction on Large Wind Turbines". *Journal of Solar Energy Engineering,* ***130***(3). 031014.

[6] Eolos wind energy research consortium. www.eolos.umn.edu/facilities/eolos-wind-research-station.

[7] Jonkman, J. M., and Buhl, M. L., 2005. Fast Users Guide. Tech. rep., National Renewable Energy Laboratory.

[8] Seiler, P., and Ozdemir, A., 2013. "An optimal time-invariant approximation for wind turbine dynamics using the multi-blade coordinate transformation". In Proc. of American Control Conference, pp. 1442–1447.

[9] Skogestad, S., and Postlethwaite, I., 2005. *Multivariable Feedback Control - Analysis and Design*. John Wiley & Sons.

[10] Glover, K., and Doyle, J., 1988. "State-space Formulae for All Stabilizing Controllers that Satisfy an $\mathscr{H}_\infty$-norm Bound and Relations to Risk Sensitivity". *Systems & Control Letters,* ***11***(3), pp. 167–172.

[11] Balas, G., Chiang, R., Packard, A., and Safonov, M. *Robust Control Toolbox User's Guide R2014b*. MathWorks.

[12] Stein, G., 2003. "Respect the unstable". *IEEE Control Systems Magazine,* ***23***(4), pp. 12–25.

[13] Blight, J., Dailey, R. L., and Gangsaas, D., 1994. "Practical control law design for aircraft using multivariable techniques". *International Journal of Control,* ***59***(1), pp. 93–137.

[14] Jonkman, B., and Kilcher, L., 2009. TurbSim User's Guide: Version 1.50. Tech. Rep. NREL/TP-500-46198, National Renewable Energy Laboratory.

[15] Buhl, M., 2008. MCrunch Users Guide for Version 1.00. Tech. Rep. NREL/TP-500-43139, National Renewable Energy Laboratory.

[16] Freebury, G., and Musial, W., 2000. "Determining equivalent damage loading for full-scale wind turbine blade fatigue tests". In Proc. 19th American Society of Mechanical Engineers Wind Energy Symposium, no. 2000-50.